Search for a Sterile Neutrino in a 3+1 Framework using the Wire-Cell Inclusive Charged-Current ν_e Selection from MicroBooNE

June 10, 2022

The MicroBooNE collaboration
microboone_info@fnal.gov

Abstract

A search for a sterile neutrino is being carried out in the MicroBooNE experiment within the 3+1 (three flavors of active neutrinos + one flavor of sterile neutrino) framework using neutrinos from the Booster Neutrino Beam (BNB) at a baseline of about 470 m with an average neutrino energy of 800 MeV. The sensitivity of this search is built upon high performance inclusive charged-current electron neutrino (ν_e) and muon neutrino (ν_μ) event selections, which were utilized in the previous search for a low-energy excess (LEE) in the ν_e energy spectrum at MicroBooNE. In this note, we present the results of a 3+1 oscillation fit considering both ν_e appearance and ν_e/ν_μ disappearance. Using the first three years' BNB data, no evidence of a light sterile neutrino was found and 95% C.L. exclusion limits were calculated in the 3+1 neutrino oscillation parameter space. Notably, the cancellation between ν_e disappearance and ν_e appearance oscillations leads to a reduced oscillation effect in the ν_e energy spectrum resulting in a degeneracy of the oscillation parameters. Such a degeneracy is expected to be mitigated by including the neutrino events from the off-axis Neutrino from the Main Injector (NuMI) beam. The prospect of a 3+1 oscillation analysis using both BNB and NuMI is reported and it is expected to considerably improve the sensitivity to 3+1 neutrino oscillations.

Contents

1 INTRODUCTION

While most neutrino oscillation results are consistent with the three-neutrino framework (see Ref. [1, 2] among others), the existence of a light eV-scale sterile neutrino has been postulated to explain several experimental anomalies. These include i) the observation that calibrated ν_e sources (^{51}Cr for GALLEX [3] and BEST [4], ^{51}Cr and ^{37}Ar for SAGE [5]) produced lower rates of measured ν_e than expected in the three-neutrino framework; ii) the reactor anti-neutrino anomaly [6], which observed a deficit in the measured $\bar{\nu}_e$ events relative to the expectation based on the reactor anti-neutrino flux calculations [7, 8]; iii) the Neutrino-4 [9] anomaly, which suggests reactor $\bar{\nu}_e$ oscillations over distances of a few meters; and iv) the anomalous excess of $\bar{\nu}_e$-like events in LSND [10] and the excess of low-energy electron-like (LEE) events in MiniBooNE [11, 12]. The above experimental results could be explained by $\nu_e/\bar{\nu}_e$ disappearance or ν_e appearance considering light sterile neutrinos. It is worth noting that such an explanation to the reactor anti-neutrino anomaly has been disfavored by recent experimental measurements [13, 14] and improved reactor neutrino flux calculations [15, 16]. Nevertheless, there are significant challenges in explaining all available experimental results with a sterile neutrino oscillation model in a global fit [17]. It is important to clarify these experimental anomalies and the sterile neutrino, if discovered, would make a profound impact on not only particle physics, but also astrophysics and cosmology.

The MicroBooNE detector [18] is a 10.4 m long, 2.6 m wide, and 2.3 m high liquid argon time projection chamber (LArTPC), located on-axis along the Booster Neutrino Beam (BNB) at the Fermi National Accelerator Laboratory in Batavia, IL, USA. It consists of approximately 85 metric tons of liquid argon in the active volume for ionization charge detection along with an array of 32 photomultiplier tubes (PMTs) [19] for the detection of scintillation light. It sits at a distance of 468.5 m from the beryllium target of the BNB, 72.5 m upstream of the MiniBooNE detector. The recent distinct and complementary low-energy excess searches at MicroBooNE [20, 21, 22, 23], which aim to provide a definite check on the MiniBooNE anomaly, conclude that "the results are found to be consistent with the nominal ν_e rate expectations from the Booster Neutrino Beam and no excess of ν_e events is observed" [20], assuming a simple LEE template unfolded from the MiniBooNE excess. While these results suggest the MiniBooNE LEE has a non-ν_e origin, the current results may still be compatible with the hypothesis of a light sterile neutrino suggested by the set of experimental anomalies mentioned above.

In order to fully evaluate the possible existence of sterile neutrinos using the MicroBooNE data, a comprehensive and sensitive 3+1 (three flavors of standard model neutrinos + one

flavor of sterile neutrino) neutrino oscillation analysis is being carried out to determine the possible parameter space allowed for sterile neutrinos. Capitalizing on the high-performance neutrino selection and systematic uncertainties of the ν_e and ν_μ event rate predictions in a recent MicroBooNE LEE analysis based on the Wire-Cell reconstruction [23], we present the 3+1 oscillation analysis results considering the oscillation effects from both ν_e appearance and ν_e/ν_μ disappearance for BNB neutrino events.

2 ANALYSIS APPROACH

This oscillation analysis utilizes the same inclusive ν_e and ν_μ charged-current (CC) channels and π^0 CC and neutral-current (NC) channels described in the published MicroBooNE Wire-Cell eLEE results [23]. The seven-channel strategy (fully contained (FC) ν_e CC , partially contained (PC) ν_e CC , FC ν_μ CC , PC ν_μ CC , FC ν_μ CC π^0 , PC ν_μ CC π^0 , and NC π^0) was kept after including the oscillation effects, where the FC events are defined to be events with the reconstructed TPC activity which is fully contained within the fiducial volume and all non-FC events are defined as PC events. These seven channels are designed to be orthogonal to each other. The inclusive ν_μ CC channel excludes ν_μ CC π^0 candidates[1]. This choice maintains the capability to apply data constraints across channels thereby reducing the systematic uncertainty in the 3+1 oscillation fit. The oscillation sensitivity is further improved by considering the oscillation effect event-by-event for the predicted signal and background events in all seven channels. The neutrino energy reconstruction[2] primarily follows a calorimetric method (sum of dE), except where track-like particles were fully-contained and longer than 4 cm, in which case the track range was used to determine the particles' kinetic energy. The energy of an electromagnetic shower from electrons or gammas is estimated by scaling the total reconstructed charge associated with the shower with an overall energy-scale calibration factor. The details of the neutrino energy reconstruction can be found in Sec. III F of Ref. [23].

The BNB Run 1-3 data consist of 6.4×10^{20} protons on target (POT), which covers the first three years' data taking (about half of the full MicroBooNE data set) was used in this analysis. MicroBooNE standard overlay Monte-Carlo (MC) samples, in which the MicroBooNE GENIE tune [24] was applied and the simulation of neutrino interactions is overlaid with dedicated beam-off data, were used. The MC samples include 1) the intrinsic ν_e and BNB ν overlay MC samples for ν_e/ν_μ disappearance events (ν_e/ν_μ to ν_e/ν_μ oscillation); 2) dedicated oscillation

---

[1]at least one π^0 reconstructed in the final state

[2]For NC events, this method essentially reconstructs the energy transfer with an invisible outgoing neutrino.

samples for ν_e appearance events (ν_μ to ν_e oscillation), whose flux systematic uncertainty comes from the BNB ν_μ flux and the cross section and detector related systematic uncertainties from ν_e interactions. In producing these samples the ν_μ appearance (ν_e to ν_μ oscillation) was ignored since the intrinsic ν_e to ν_μ ratio is about 0.6% and so, ν_e to ν_μ oscillations would produce an insignificant difference to the total number of observed ν_μ events.

2.1 Oscillation Model

We use a 3+1 neutrino framework with the 4×4 (4 flavors by 4 mass eigenstates) unitary PMNS matrix parameterized as below [25]

$$U = R_{34}(\theta_{34},\delta_{34})R_{24}(\theta_{24},\delta_{24})R_{14}(\theta_{14},0)R_{23}(\theta_{23},0)R_{13}(\theta_{13},\delta_{13})R_{12}(\theta_{12},0), \tag{1}$$

where $R_{ij}(\theta_{ij},\delta_{ij})$ denotes a counterclockwise rotation in the complex ij-plane through a mixing angle θ_{ij} and a CP phase δ_{ij}. Assuming the postulated fourth neutrino mass eigenstate is much heavier than the others ($m_4 \gg m_3, m_2, m_1$), the short-baseline oscillation probability from α-flavor to β-flavor neutrinos in vacuum can be expressed as

$$P_{\nu_\alpha \to \nu_\beta} = \delta_{\alpha\beta} + (-1)^{\delta_{\alpha\beta}} \cdot \sin^2 2\theta_{\alpha\beta} \cdot \sin^2 \Delta_{41}, \tag{2}$$

where

$$\Delta_{41} \equiv \frac{\Delta m_{41}^2 L}{4E} = 1.267 \left(\frac{\Delta m_{41}^2}{\text{eV}^2}\right)\left(\frac{\text{MeV}}{E}\right)\left(\frac{L}{m}\right), \tag{3}$$

$\delta_{\alpha\beta}$ is the Kronecker delta, and $\theta_{\alpha\beta}$ is defined as the effective mixing angle.

Table 1 shows the connection between the effective mixing angles and the PMNS matrix elements. There are four independent oscillation parameters: Δm_{41}^2, $\sin^2\theta_{14}$, $\sin^2\theta_{24}$, and $\sin^2\theta_{34}$ to describe the mixing of electron (e) neutrinos, muon (μ) neutrinos, tau (τ) neutrinos, and postulated light sterile (s) neutrinos.

$\sin^2 2\theta_{ee}$	$= \sin^2 2\theta_{14}$	$= 4(1-|U_{e4}|^2)|U_{e4}|^2$
$\sin^2 2\theta_{\mu\mu}$	$= 4\cos^2\theta_{14}\sin^2\theta_{24}\left(1-\cos^2\theta_{14}\sin^2\theta_{24}\right)$	$= 4(1-|U_{\mu4}|^2)|U_{\mu4}|^2$
$\sin^2 2\theta_{\mu e}$	$= \sin^2 2\theta_{14}\sin^2\theta_{24}$	$= 4|U_{\mu4}|^2|U_{e4}|^2$
$\sin^2 2\theta_{es}$	$= \sin^2 2\theta_{14}\cos^2\theta_{24}\cos^2\theta_{34}$	$= 4|U_{e4}|^2|U_{s4}|^2$
$\sin^2 2\theta_{\mu s}$	$= \cos^4\theta_{14}\sin^2 2\theta_{24}\cos^2\theta_{34}$	$= 4|U_{\mu4}|^2|U_{s4}|^2$

Table 1: Definition of the 3+1 effective oscillation angles using the parameterized PMNS matrix as shown in Eq. 1. 's' denotes the postulated light sterile neutrinos.

2.2 Oscillation Fit

In the 3+1 oscillation parameter fit, we adopt the covariance matrix formalism to construct the χ^2 test statistic:

$$\chi^2 = (M - P(\boldsymbol{\theta}))^T \times Cov_{full}^{-1}(M, P(\boldsymbol{\theta})) \times (M - P(\boldsymbol{\theta})), \tag{4}$$

where $\boldsymbol{\theta}$ represents the oscillation parameters, M and P are vectors of the measurements and the predictions for the seven channels, respectively. The Cov_{full} is the full covariance matrix:

$$Cov_{\text{full}} = Cov_{\text{CNP}}^{\text{stat}} + Cov_{\text{MC,stat}}^{\text{sys}} + Cov_{\text{flux}}^{\text{sys}} + Cov_{\text{xsec}}^{\text{sys}} + Cov_{\text{det}}^{\text{sys}}, \tag{5}$$

where $Cov_{\text{CNP}}^{\text{stat}}$ is the statistical covariance matrix following the Combined-Neyman-Pearson (CNP) formalism [26] with the diagonal elements corresponding to $3/(1/M_i + 2/P_i)$ for the ith bin. $Cov_{\text{MC,stat}}^{\text{sys}}$ is a diagonal covariance matrix accounting for the statistical fluctuation in making the MC central value prediction. The other three covariance matrices $Cov_{\text{flux}}^{\text{sys}}$, $Cov_{\text{xsec}}^{\text{sys}}$, and $Cov_{\text{det}}^{\text{sys}}$ are the covariance matrices corresponding to the neutrino flux, cross section[3], and detector response systematic uncertainties, respectively. Details of the estimation of these covariance matrices can be found in Sec. V of Ref. [23].

The prediction $P(\boldsymbol{\theta})$ and the covariance matrix $Cov(M, P(\boldsymbol{\theta}))$ both depend on the oscillation parameters, $\boldsymbol{\theta}$, in the χ^2 minimization. Given a set of $\boldsymbol{\theta}$, the oscillation effect is applied as an event weight to each event based on its baseline, true neutrino energy, initial and final neutrino flavors, and the interaction type. For NC interactions, we apply an oscillation probability $1 - P_{\nu_e \to \nu_s}$ for ν_e events and $1 - P_{\nu_\mu \to \nu_s}$ for ν_μ events. We fix θ_{34} at zero ($\cos^2\theta_{34} = 1$) for NC events as it has a negligible impact on this analysis. Therefore, the actual oscillation parameters in the fit are Δm_{41}^2, $\sin^2\theta_{14}$, and $\sin^2\theta_{24}$. The $\sin^2 2\theta_{ee}$ and $\sin^2 2\theta_{\mu e}$ mixing parameters obtained from the 3+1 oscillation analysis are converted from the two mixing angles following the formula shown in table 1. We vary the systematic uncertainty $Cov^{\text{sys}}(P(\boldsymbol{\theta}))$ for different oscillation parameters via the fractional covariance matrix approach "$Cov_{ij} = P_i \cdot F_{ij} \cdot P_j$" where P is the prediction as a function of oscillation parameters and F is the fractional covariance matrix, which is decoupled from the total number of events in each bin. F was found to have a negligible dependence on the oscillation parameters and is assumed to be constant in our calculation.

---

[3]Includes both neutrino-argon scattering cross section and final-state hadron-argon interaction cross section.

2.3   Setting an exclusion upper limit

In the absence of a discovery of new physics beyond the 3ν hypothesis, the CLs method [27, 28] is used to set the limits of oscillation parameters based on the χ^2 defined in Eq. 4. The CLs method is essentially a two-hypothesis test that compares a 4ν hypothesis to the 3ν hypothesis. We use the test statistic

$$\Delta\chi^2(x) = \chi^2_{4\nu}(x) - \chi^2_{3\nu}(x), \tag{6}$$

to determine if a 4ν hypothesis can be excluded at a certain confidence level. $\chi^2_{4\nu}(x)$ is the χ^2 value of the measurement x with the prediction from a given set of 4ν oscillation parameters, and $\chi^2_{3\nu}(x)$ is the χ^2 value corresponding to the 3ν hypothesis. The CL_s is then defined as

$$\mathrm{CL}_s = \frac{\mathrm{CL}_{s+b}}{\mathrm{CL}_b}, \tag{7}$$

$$\mathrm{CL}_{s+b} = \mathrm{Prob}(\Delta\chi^2 \geq \Delta\chi^2_{\mathrm{obs}}|4\nu), \tag{8}$$

$$\mathrm{CL}_b = \mathrm{Prob}(\Delta\chi^2 \geq \Delta\chi^2_{\mathrm{obs}}|3\nu), \tag{9}$$

where CL_{s+b} and CL_b are the p-values (right-tail probability) of the observed $\Delta\chi^2_{\mathrm{obs}}$ when the 4ν or 3ν hypothesis is true. The region with $\mathrm{CL}_s \leq 1 - \alpha$ is excluded at the confidence level of α. By throwing pseudo-experiments corresponding to a 3ν or 4ν hypothesis, the distribution of $\Delta\chi^2$ as defined in Eq. 6 can be obtained, as illustrated in figure 1, therefore the CL_{s+b} and CL_b can be calculated for a given $\Delta\chi^2_{\mathrm{obs}}$ value either from data or a pseudo-experiment. We refer to this as the "frequentist CLs method".

When the statistical and systematic uncertainties are small enough [29], the distribution of $\Delta\chi^2$ as defined in Eq. 6 asymptotically follows a Gaussian distribution with $\mu = \Delta\chi^2(x = \mathrm{Asimov\ dataset})$ and $\sigma = 2\sqrt{\mu}$. Hence, Eq. 7 can be approximated to be

$$\mathrm{CL}_s \approx \frac{1 + \mathrm{Erf}\left(\frac{\Delta\chi^2(4\nu\ \mathrm{Asimov}) - \Delta\chi^2(x)}{\sqrt{8|\Delta\chi^2(4\nu\ \mathrm{Asimov})|}}\right)}{1 + \mathrm{Erf}\left(\frac{\Delta\chi^2(3\nu\ \mathrm{Asimov}) - \Delta\chi^2(x)}{\sqrt{8|\Delta\chi^2(3\nu\ \mathrm{Asimov})|}}\right)}, \tag{10}$$

where in our case the Asimov dataset[4] [30] corresponds to the central value prediction for a given hypothesis without any fluctuations. We call this the "Gaussian CL_s method" [29]. The Gaussian approximation is invalid when the statistical and/or systematic uncertainty is

---

[4]The Asimov dataset is such that when one uses it to evaluate the estimator for all parameters, one obtains the true parameter values.
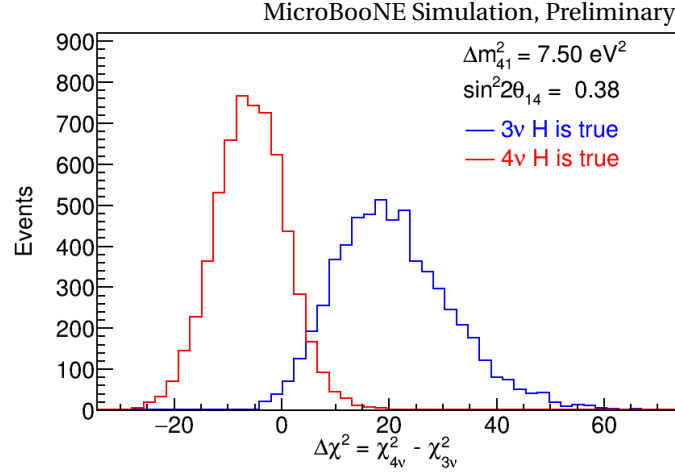
Figure 1: $\Delta\chi^2$ distribution from pseudo-experiments assuming the 4ν hypothesis (red) or the 3ν hypothesis (blue) is true. The results are from the oscillation parameters at (7.50 eV^2, 0.38) of $(m^2_{41}, \sin^2 2\theta_{14})$.

relatively large[5]. By default we use the frequentist CL$_s$ method to calculate the sensitivity and set the exclusion upper limit for data. To illustrate the potential improvement of sensitivity combining both BNB and NuMI data (Sec. 4), the Gaussian CL$_s$ method with Asimov datasets is used as it is computationally inexpensive and shows reasonable consistency with the frequentist CL$_s$ method median sensitivity (e.g. figure 6 sensitivity versus figure 12 sensitivity with $\sin^2\theta_{24} = 0.005$).

3   RESULTS FROM BNB

In a 3+1 oscillation analysis, both ν_e appearance and ν_e/ν_μ disappearance are considered. The ν_e disappearance can cancel the appearance of ν_e events resulting in a degeneracy of the oscillation parameters as shown in the following equation

$$N_{\nu_e} = N_{\text{intrinsic } \nu_e} \cdot P_{\nu_e \to \nu_e} + N_{\text{intrinsic } \nu_\mu} \cdot P_{\nu_\mu \to \nu_e} \tag{11}$$

$$= N_{\text{intrinsic } \nu_e} \cdot \left[1 + (R_{\nu_\mu/\nu_e} \cdot \sin^2\theta_{24} - 1) \cdot \sin^2 2\theta_{14} \cdot \sin^2\Delta_{41} \right] \tag{12}$$

where R_{ν_μ/ν_e} is the ratio of intrinsic ν_μ and ν_e events and this equation is for ν_e of a given true neutrino energy. In the case of BNB only, the degeneracy of $\sin^2\theta_{24}$ and $\sin^2 2\theta_{14}$ happens when $\sin^2\theta_{24}$ approaches $1/\bar{R}^{\text{BNB}}_{\nu_\mu/\nu_e} \approx 0.005$. Figure 2 illustrates the energy spectra of the ν_e CC

---

[5]A large systematic uncertainty here means either large in magnitude or with large bin-to-bin correlations.

fully contained events at different values of the oscillation parameters corresponding to no oscillation effect and characteristic 4ν oscillation parameters referencing the Neutrino-4 best-fit values. The yellow and blue curves show obvious oscillation effects, but the red curve shows a weak oscillation effect below 1500 MeV due to the cancellation between ν_e disappearance and appearance. Red dashed and red solid curves show that the ν_e CC energy spectra are insensitive to oscillations when $\sin^2\theta_{24}$ is at 0.005. Given this degeneracy around $\sin^2\theta_{24}$=0.005, the best-fit of (Δm_{41}^2, $\sin^2\theta_{14}$, $\sin^2\theta_{24}$) could be especially biased when the best-fit $\sin^2\theta_{24}$ is close to this degeneracy point which manifests as a local minimum of the χ^2 distribution in the oscillation parameter space. Meanwhile, the sensitivity around this region gets worse.
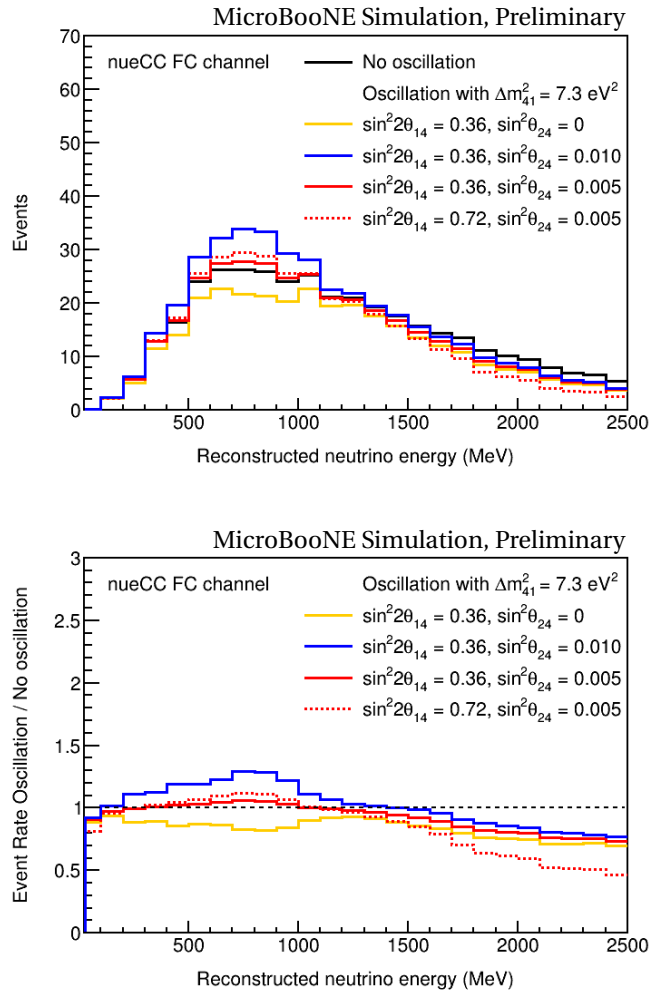

Figure 2: Energy spectra of the selected ν_e CC fully contained events at different values of the oscillation parameters.

The simultaneous fit of $(\Delta m_{41}^2, \sin^2\theta_{14}, \sin^2\theta_{24})$ using the 7 channels gives a data best-fit result of (1.295, 0.936, 0) with a $\chi_{\min}^2(\text{data})/\text{ndf}=86.62/179$. The best-fit value of $\sin^2\theta_{14}$ corresponds to $\sin^2 2\theta_{14} = 0.240$. In comparison, assuming the 3ν hypothesis is true, the $\chi_{3\nu}^2(\text{data})/\text{ndf}$ is equal to 89.15/182. In this fit, the initial values of the oscillation parameters are obtained by scanning a 3-D grid of $60 \times 60 \times 60$ points that are evenly distributed in a log-scale from 0.1-100 eV^2, 0.0001-1.0, and 0.0001-1.0 for Δm_{41}^2, $\sin^2\theta_{14}$, and $\sin^2\theta_{24}$, respectively. The initial values correspond to the grid point which gives the minimal χ^2 relative to the others. The final best-fit values are obtained by float parameter minimization using MINUIT. Figure 3 and figure 4 show the energy spectra of the data, the 3ν prediction (after constraints from ν_μ CC , CC π^0 and NC π^0 channels), and the best-fit 4ν prediction for the 7 channels and the ν_e CC channels, respectively. The compatibility between the data and the 3ν hypothesis is quantitatively calculated using the Feldman-Cousins approach [31]. The p-value of the data for the 3ν hypothesis is found to be 0.426 by comparing $\chi_{3\nu}^2(\text{data})$-$\chi_{\min}^2(\text{data})=2.53$ with the distribution of $\Delta\chi_{\text{FC}}^2$ (= $\chi_{3\nu}^2 - \chi_{\min}^2$). Figure 5 shows the $\Delta\chi_{\text{FC}}^2$ distribution from two thousands of pseudo-experiments assuming the 3ν hypothesis is true. The data result ($\Delta\chi^2(\text{data}) = 2.53$) is also shown in the same figure. The p-value indicates a good compatibility between the data and the 3ν hypothesis, which are consistent within 1σ. We'll report the CL$_s$ exclusion upper limits from the data.

Bin index	Channel	Energy range (GeV)	Bin width (GeV)	Kinematic type
0-24	FC ν_e CC	0.0-2.5	0.1	neutrino energy
25	FC ν_e CC	$\geq$2.5	-	neutrino energy
26-50	PC ν_e CC	0.0-2.5	0.1	neutrino energy
51	PC ν_e CC	$\geq$2.5	-	neutrino energy
52-76	FC ν_μ CC	0.0-2.5	0.1	neutrino energy
77	FC ν_μ CC	$\geq$2.5	-	neutrino energy
78-102	PC ν_μ CC	0.0-2.5	0.1	neutrino energy
103	PC ν_μ CC	$\geq$2.5	-	neutrino energy
104-128	FC ν_μ CC π^0	0.0-2.5	0.1	neutrino energy
129	FC ν_μ CC π^0	$\geq$2.5	-	neutrino energy
130-154	PC ν_μ CC π^0	0.0-2.5	0.1	neutrino energy
155	PC ν_μ CC π^0	$\geq$2.5	-	neutrino energy
156-180	NC π^0	0.0-2.5	0.1	energy transfer
181	NC π^0	$\geq$2.5	-	energy transfer

**Table 2:** Definition of bin indices in figure 3.

The results considering a full 3 active neutrinos + 1 sterile neutrino oscillation scenario are shown below. Figure 6 and figure 7 show the 95% C.L. exclusion limits in the 2D parameter

MicroBooNE 6.369×10^{20} POT, Preliminary
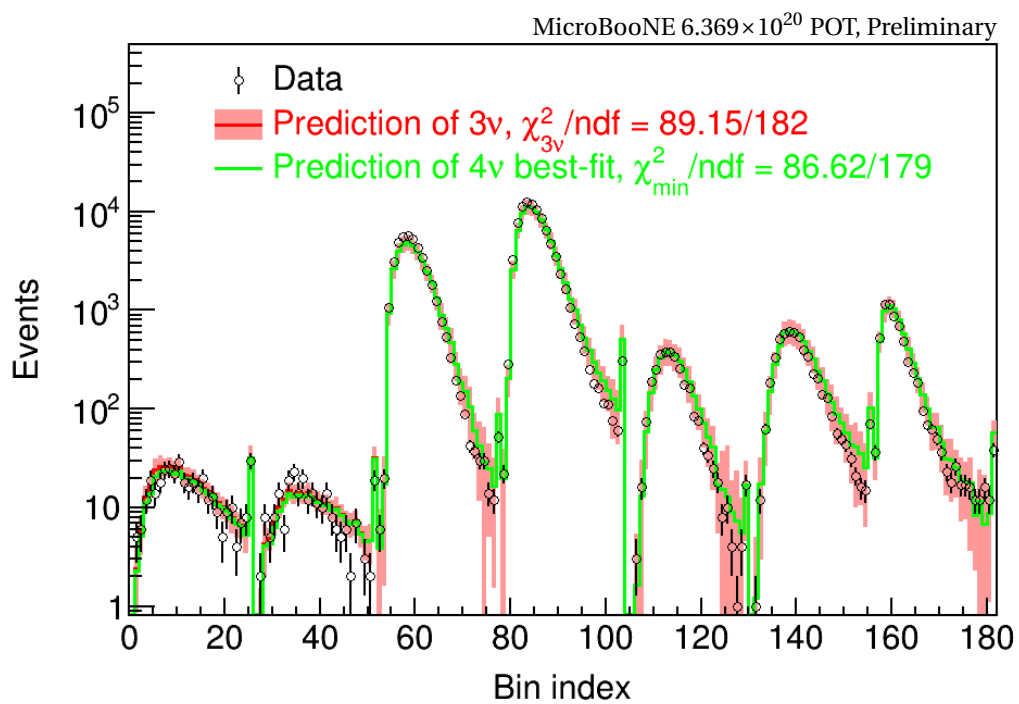
Figure 3: Energy spectra of the 7 channels: data (black circle), prediction of 3ν hypothesis (red curve), and prediction from the best fit of 4ν hypothesis (green curve). The error bar on each data point represents the statistical uncertainty. The red band on the prediction represents the systematic uncertainty. Definition of bin indices can be found in table 2.
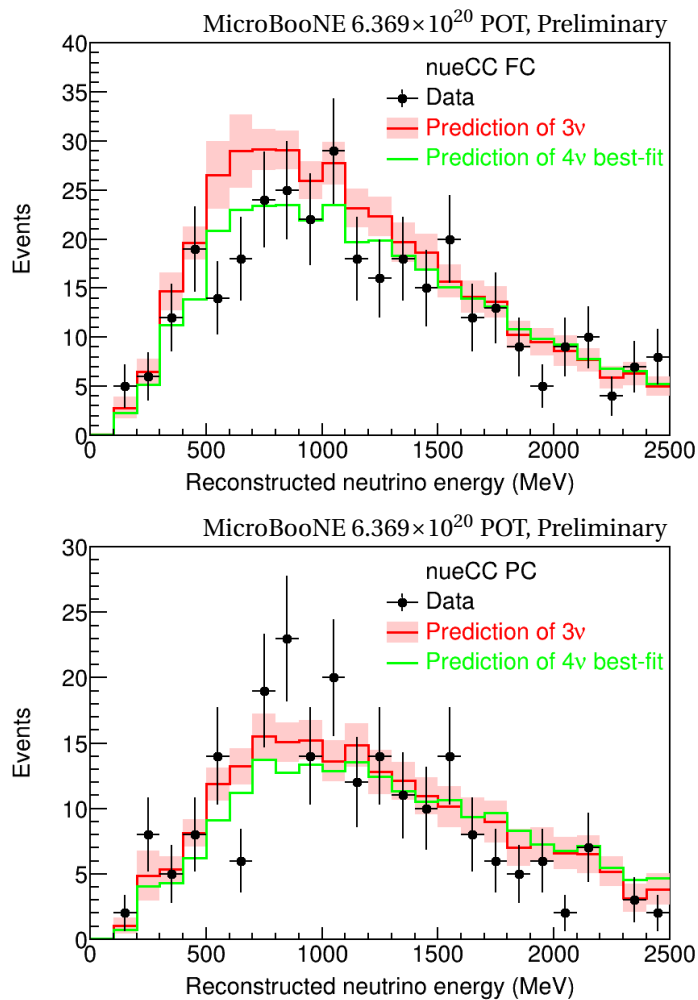
Figure 4: Energy spectra of the ν_e CC FC channel (top) and PC channel (bottom): data (black circle), prediction of the 3ν hypothesis (red curve) after constraints from ν_μ CC , CC π^0 and NC π^0 channels, and the prediction of the best fit 4ν hypothesis (green curve). The error bar on each data point represents the statistical uncertainty. The red band on the prediction represents the systematic uncertainty. These two figures are zoom-in figures from figure 3.
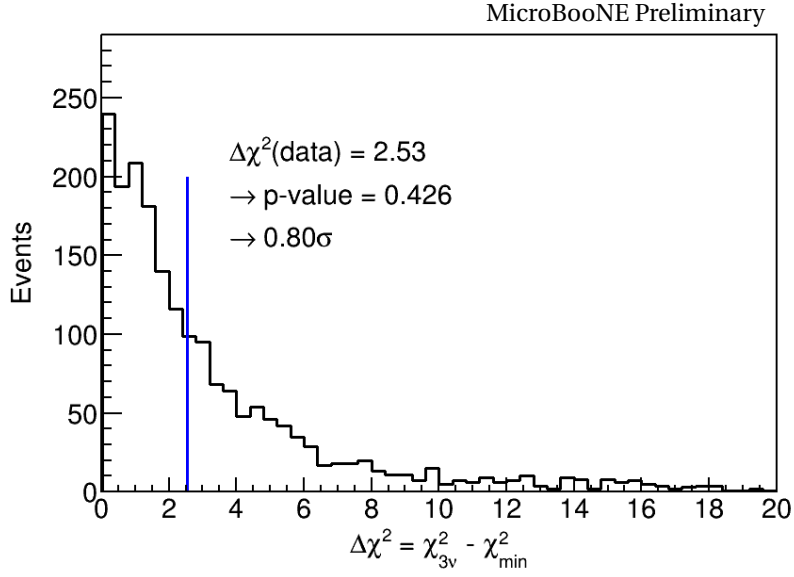
Figure 5: Distribution of $\Delta\chi^2$ assuming 3ν hypothesis is true. The data $\Delta\chi^2$(data) value is indicated by the blue vertical line. The data measurement has a p-value of 0.426 for the test statistic from the 3ν hypothesis pseudo-experiments, corresponding to only a 0.80σ discrepancy.

space of Δm^2_{41} vs. $\sin^2 2\theta_{ee}$ and Δm^2_{41} vs. $\sin^2 2\theta_{\mu e}$. Both sensitivity and data results are from the frequentist CL$_s$ method. No obvious inconsistency was found in data compared to the sensitivity. In figure 6 the data result allows slightly more oscillation phase space due to the overall deficit we observed in the ν_e CC channel. In figure 7 the sensitivity curve ends at $\sin^2 2\theta_{\mu e}$=0.005 because $\sin^2 2\theta_{\mu e}$ is equal or less than $\sin^2 \theta_{24}$ which is fixed at 0.005. The data exclusion limit is a 2D profiled result obtained by minimizing over $\sin^2 \theta_{24}$ at each point of the 2D parameter space. The sensitivity result (1σ and 2σ bands) corresponds to $\sin^2 \theta_{24}$ fixed at 0.005, for which we expect to have the least sensitive 2D projected sensitivity[6] because of maximum parameter degeneracy at this $\sin^2 \theta_{24}$ value.

Figure 8 shows the comparisons of our result with the allowed regions of Neutrino-4 [9] and gallium anomaly [4] results in the Δm^2_{41} vs. $\sin^2 2\theta_{ee}$ parameter space. The Neutrino-4 and gallium experiments have no ν_μ events from their neutrino sources, and their results correspond to a full 3+1 oscillation scenario that effectively nue disappearance only measurements. For MicroBooNE, especially in this study, both ν_e and ν_μ events from the BNB beam are used and the result (solid red curve; 2D profiling) corresponds to a full 3+1 oscillation analysis considering both ν_e appearance and ν_e /ν_μ disappearance. In comparison, the MicroBooNE ν_e disappearance only result (dashed green curve) corresponding to $\sin^2\theta_{24}$=0 is

---

[6]The least sensitive result is more suitable to be compared to the 2D profiled result.

also presented, which provides a more stringent limit than the full 3+1 oscillation result, as expected. A fraction of the Neutrino-4 and gallium anomaly allowed regions are excluded by this analysis result at 95% CL. With the addition of NuMI data (see Sec. 4), the physics sensitivity can be extended covering the full Neutrino-4 and gallium anomaly 2σ allowed region as indicated by the dashed magenta curve in figure 8. This BNB+NuMI sensitivity was calculated based on about 50% and 20% of the full MicroBooNE BNB and NuMI datasets, in the full 3+1 oscillation scenario with $\sin^2\theta_{24}$ at 0.005.
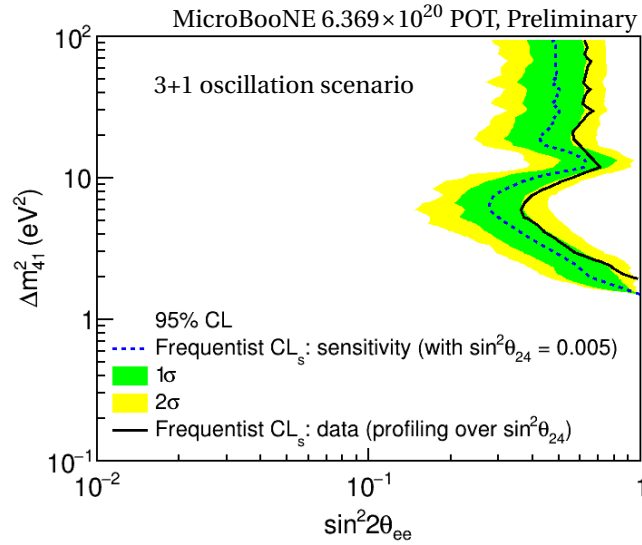

Figure 6: MicroBooNE 95% C.L. exclusion limit in the 2D parameter space of Δm_{41}^2 vs. $\sin^2 2\theta_{ee}$. Both sensitivity (fixed $\sin^2\theta_{24}$ at 0.005) and data (2D profiling by minimizing over $\sin^2\theta_{24}$) results are from the frequentist CL$_s$ method in the full 3+1 neutrino oscillation scenario. For each Δm_{41}^2, the frequentist CL$_s$ sensitivity curve corresponds to the median (50% quantile) value and the green and yellow bands correspond to $(50\pm68.3/2)$% and $(50\pm95.5/2)$% quantiles in the distribution of 95% C.L. exclusion limits from 3ν pseudo-experiments.

Figure 9 shows the comparisons of our result with the allowed region of LSND [10] in the Δm_{41}^2 vs. $\sin^2 2\theta_{\mu e}$ parameter space. The LSND result is for a $\bar{\nu}_e$ appearance only oscillation analysis with low intrinsic $\bar{\nu}_e$ background, on which the impact of $\bar{\nu}_e$ disappearance is insignificant. The MicroBooNE full 3+1 neutrino oscillation result (solid red curve) considering both ν_e appearance and ν_e/ν_μ disappearance are reported. In comparison, the ν_e appearance only result (dashed green curve), which is not allowed in the 3+1 neutrino oscillation framework, is also presented. Part of the LSND allowed region is excluded by the full 3+1 oscillation analysis result at 95% CL. With the addition of NuMI data (see Sec. 4), the physics sensitivity can be extended covering the full LSND 99% CL allowed region as indicated by the dashed magenta curve in figure 9. This BNB+NuMI sensitivity was calculated based on about 50%
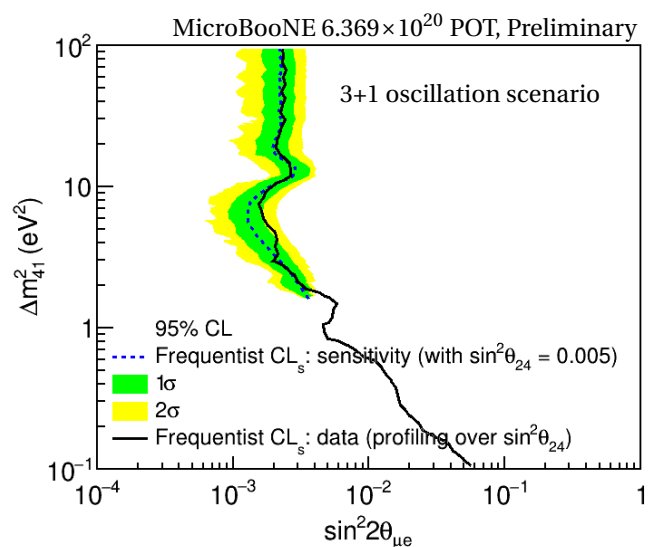
Figure 7: MicroBooNE 95% C.L. exclusion limit in the 2D parameter space of Δm^2_{41} vs. $\sin^2 2\theta_{\mu e}$. Both sensitivity (fixed $\sin^2 \theta_{24}$ at 0.005) and data (2D profiling by minimizing over $\sin^2 \theta_{24}$) results are from the frequentist CL_s method in the full 3+1 neutrino oscillation scenario. For each Δm^2_{41}, the frequentist CL_s sensitivity curve corresponds to the median (50% quantile) value and the green and yellow bands correspond to $(50\pm68.3/2)\%$ and $(50\pm95.5/2)\%$ quantiles in the distribution of 95% C.L. exclusion limits from 3ν pseudo-experiments. The sensitivity curve ends at $\sin^2 2\theta_{\mu e}$=0.005 because $\sin^2 2\theta_{\mu e}$ is equal or less than $\sin^2 \theta_{24}$ which is fixed at 0.005 in the sensitivity calculation.
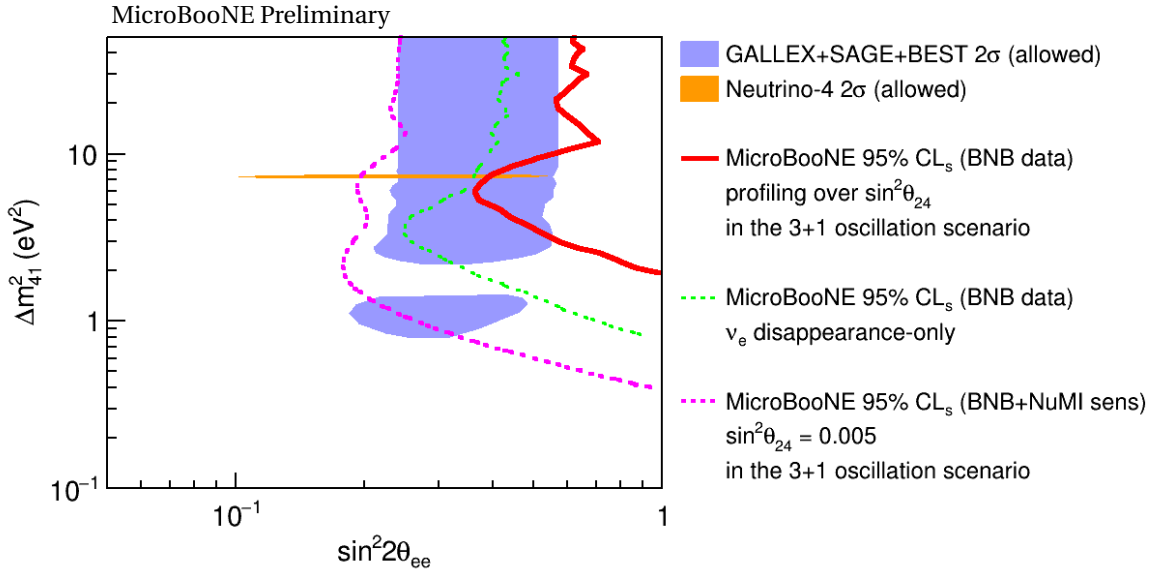
Figure 8: MicroBooNE 95% confidence level frequentist CL_s limits in the Δm_{41}^2 vs. $\sin^2 2\theta_{ee}$ parameter space. The GALLEX+SAGE+BEST [4] and Neutrino-4 [9] 2σ allowed regions are shown in the shaded areas. The red solid curve represents the MicroBooNE 95% CL_s exclusion limit (2D profiling by minimizing over $\sin^2\theta_{24}$) in the full 3+1 neutrino oscillation scenario (both ν_e appearance and ν_e/ν_μ disappearance) using BNB Run 1-3 data. The green dashed curve represents the data exclusion limit in the ν_e disappearance-only scenario as opposed to the full 3+1 oscillation result. The magenta dashed curve represents the MicroBooNE 95% CL_s sensitivity in the full 3+1 oscillation scenario with a fixed $\sin^2\theta_{24}$ at 0.005 when both BNB and NuMI data are combined. This sensitivity is calculated based on the Gaussian approximation CL_s method which is computationally inexpensive and the result is similar to the frequentist CL_s median sensitivity. BNB data correspond to the Run 1-3 data-taking period with a data exposure of 6.369×10^{20} POT, and NuMI data correspond to the Run 1 data-taking period with a data exposure of 1.917×10^{20} POT.
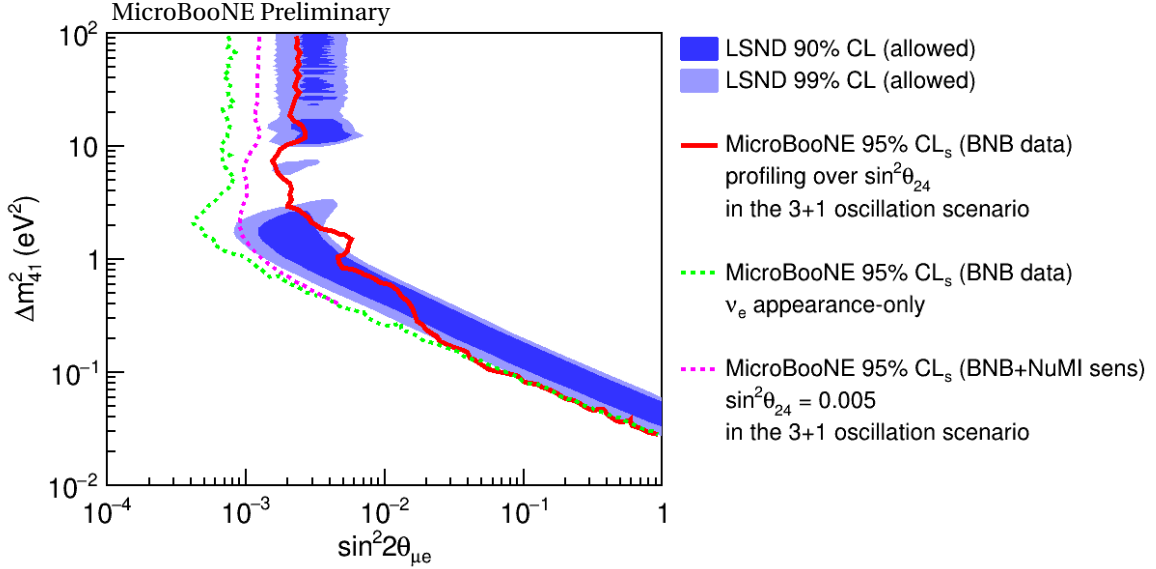
Figure 9: MicroBooNE 95% confidence level frequentist CL_s limits in the Δm_{41}^2 vs. $\sin^2 2\theta_{\mu e}$ parameter space. The LSND 90% and 99% CL allowed regions [10] are shown in the shaded areas. The LSND result is for a $\bar{\nu}_e$ appearance only oscillation analysis with low intrinsic $\bar{\nu}_e$ background, on which the impact of $\bar{\nu}_e$ disappearance is insignificant. The red solid curve represents the MicroBooNE 95% CL_s exclusion limit (2D profiling by minimizing over $\sin^2\theta_{24}$) in the full 3+1 neutrino oscillation scenario (both ν_e appearance and ν_e / ν_μ disappearance) using BNB Run 1-3 data. The green dashed curve represents the data exclusion limit in the ν_e appearance only scenario (physically not allowed by the 3+1 oscillation framework) as opposed to the full 3+1 oscillation result. The magenta dashed curve represents the MicroBooNE 95% CL_s sensitivity in the full 3+1 oscillation scenario of a fixed $\sin^2\theta_{24}$ at 0.005 when both BNB and NuMI data are combined. This sensitivity is calculated based on the Gaussian approximation CL_s method which is computationally inexpensive and the result is similar to the frequentist CL_s median sensitivity. BNB data correspond to the Run 1-3 data-taking period with a data exposure of 6.369×10^{20} POT, and NuMI data correspond to the Run 1 data-taking period with a data exposure of 1.917×10^{20} POT.

and 20% of the full MicroBooNE BNB and NuMI datasets, in the full 3+1 oscillation scenario with $\sin^2\theta_{24}$ at 0.005. With the same caveats with respect to the ν_e appearance only versus full 3+1 oscillation analyses, the MicroBooNE 3+1 results also exclude parts of the MiniBooNE allowed regions [32] which assumes the origin of the low-energy excess is solely due to ν_e.

Although the main results in this note are for the full 3+1 oscillation analysis, results for the simplified scenarios of ν_e disappearance only, ν_e appearance only, and ν_μ disappearance only can also be found in the appendix.

# 4 PROSPECT OF USING BOTH BNB AND NuMI DATA

In this section, the prospect of the addition of NuMI (Neutrino at the Main Injector) data in this 3+1 oscillation analysis is presented.

Figure 10 shows that the intrinsic flux and ν_μ to ν_e ratio in NuMI is quite different from that in BNB. The addition of NuMI events in the 3+1 oscillation helps to break the degeneracy of the oscillation parameters. Figure 11 shows the energy spectra of the selected ν_e CC fully contained events at different values of the oscillation parameters for BNB and NuMI, respectively.
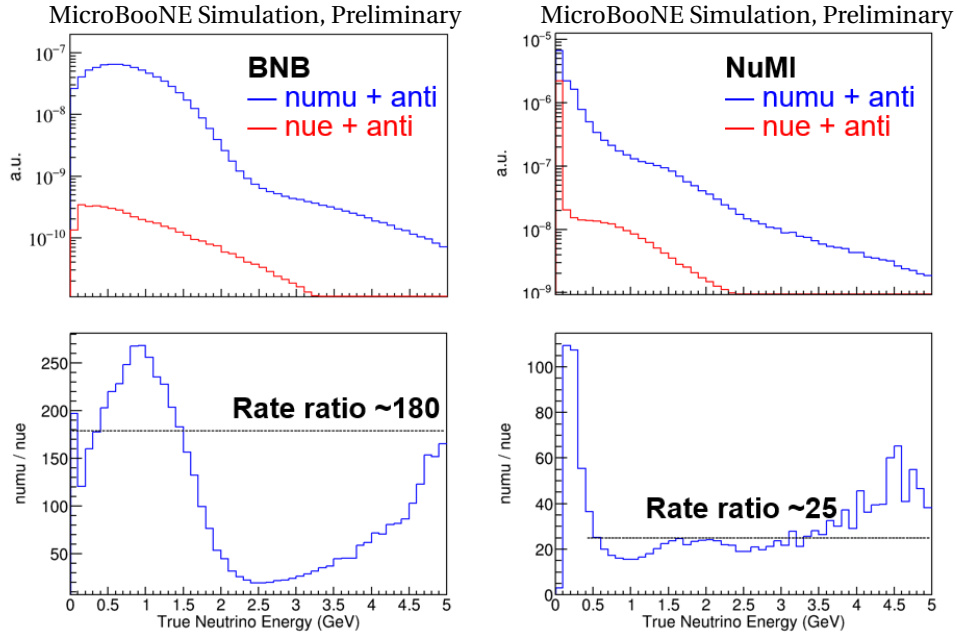

Figure 10: BNB and NuMI intrinsic ν_e and ν_μ flux and their ratios as a function of true neutrino energy.

Because the NuMI degeneracy point is around $\sin^2\theta_{24} \sim 0.04$ which is far away from the BNB degeneracy point, the addition of NuMI data can significantly reduce the BNB degeneracy. The BNB+NuMI sensitivity compared to the BNB only result is expected to have a weak dependence on $\sin^2\theta_{24}$ rather than a local minimum (which leads to worse sensitivity) around $\sin^2\theta_{24} \sim 0.005$. The NuMI data can also provide more statistics of ν events, particularly the ν_e events. For example, the NuMI Run 1 sample provides a similar amount of ν_e CC events as BNB Run 1-3. In addition, the NuMI neutrinos also extend the range of L/E values, which would increase sensitivity to a broader parameter space. Figure 12 shows the comparison of BNB-only (Run 1-3) and BNB+NuMI (BNB Run 1-3 and NuMI Run 1) sensitivity results for $\sin^2 2\theta_{14}$ for different $\sin^2\theta_{24}$ values. The BNB+NuMI sensitivity is significantly improved and
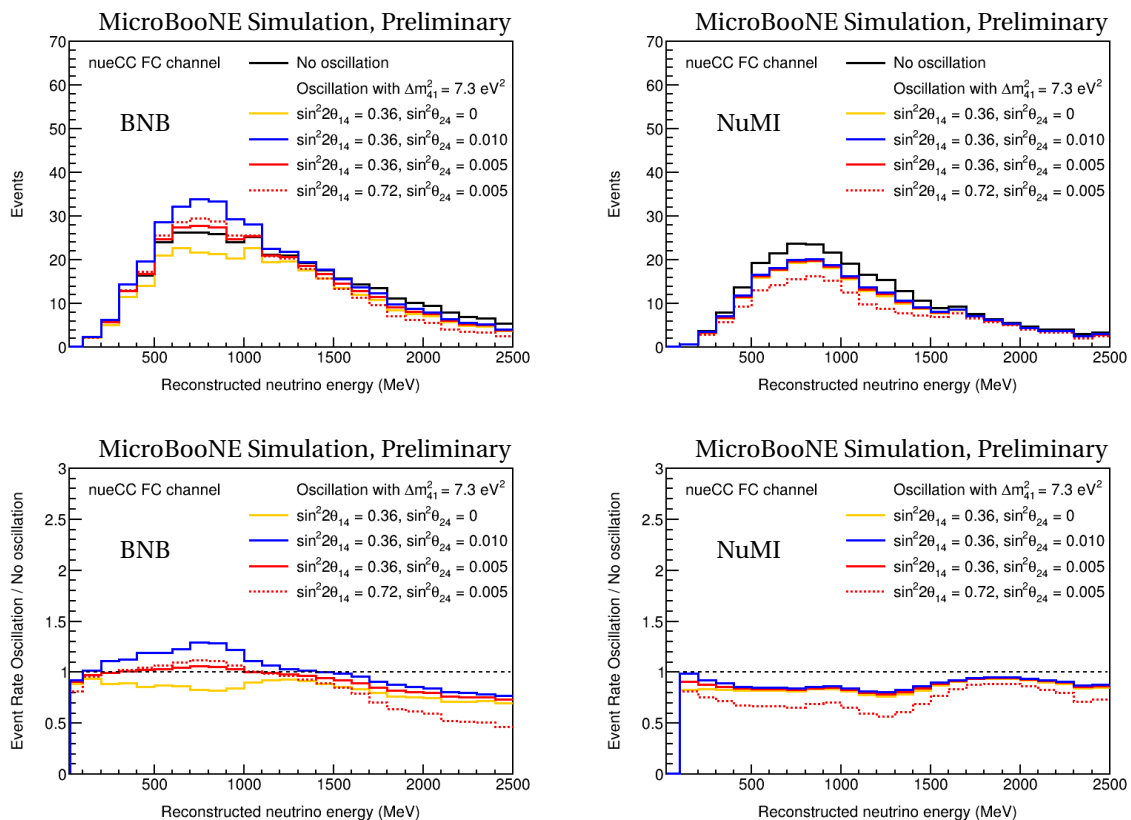
Figure 11: Energy spectra of the selected events from BNB (left) and NuMI (right) in the ν_e CC FC channel at different values of oscillation parameters.

has largely reduced degeneracy around $\sin^2\theta_{24} \sim 0.005$ compared to the BNB only result.
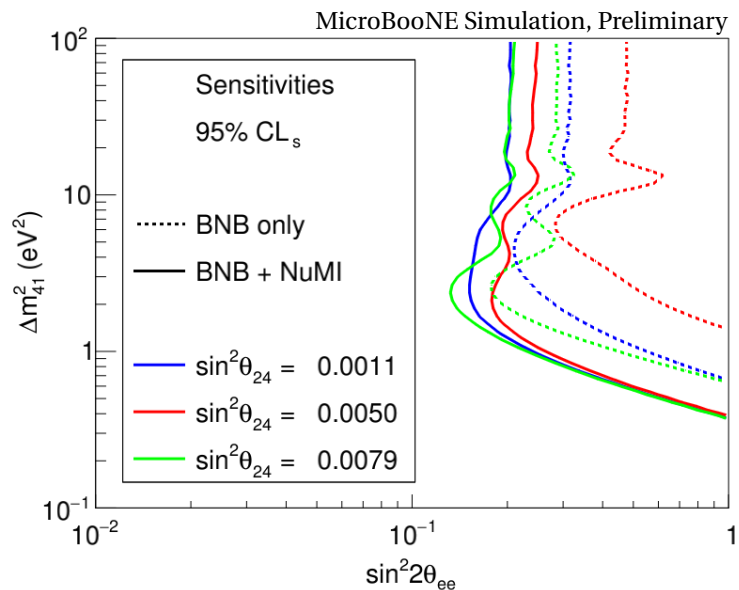
Figure 12: Sensitivities (Gaussian approximation CLs method) at 95% confidence level for the full 3+1 oscillation scenario (ν_e appearance + ν_e/ν_μ disappearance) at different $\sin^2\theta_{24}$ values. Dashed curves correspond to BNB only results. BNB data correspond to the Run 1-3 data-taking period with a data exposure of 6.369×10^{20} POT, and NuMI data correspond to the Run 1 data-taking period with a data exposure of 1.917×10^{20} POT.

5 SUMMARY

In this note, we present the 3+1 sterile neutrino oscillation analysis results using the BNB seven-channel selections which were developed and applied in the Wire-Cell eLEE analysis [23]. We report the best-fit result for the three oscillation parameters (Δm_{41}^2, $\sin^2\theta_{14}$, $\sin^2\theta_{24}$) that dictate short-baseline 3+1 neutrino oscillations. Considering the full 3+1 oscillation, the data result is consistent with the 3ν hypothesis within 1σ following the Feldman-Cousins approach. Exclusion upper limits of the several effective mixing angles and the mass-squared difference for a postulated light sterile neutrino are calculated and compared to the sensitivity results. Data exclusion upper limits and sensitivity results in the simplified ν_e disappearance or ν_e appearance scenarios are shown as well which are generally more stringent than the full 3+1 oscillation results. In summary,

- The MicroBooNE data are consistent with the 3ν hypothesis and provide no evidence for a sterile neutrino.

- The MicroBooNE exclusion limits cover a large fraction of sterile neutrino parameter space allowed by results from other experiments.

In the future, we plan to add the NuMI events and do a combined BNB+NuMI oscillation analysis to mitigate the degeneracy of oscillation parameters. More data from the BNB and/or NuMI will also be included with other advancements in neutrino flavor identification and energy reconstruction to further improve the physics sensitivity to 3+1 neutrino oscillations.

Appendices

## RESULTS FROM SIMPLIFIED OSCILLATION SCENARIOS

In this appendix, the ν_e disappearance only (ν_e to ν_e oscillation), ν_e appearance only (ν_μ to ν_e oscillation), and ν_μ disappearance only (ν_μ to ν_μ oscillation) results are reported. The results can be compared to those in Ref. [33] that were calculated based on the MicroBooNE LEE data release. To first order, these results should be consistent ignoring the impact of a precise L/E determination and energy smearing for each MC event. Moreover, we set the exclusion upper limit using a frequentist approach to properly take into account low statistics and large systematic uncertainties in the neutrino selections.

Figure 13 shows the exclusion and sensitivity contours in the Δm^2_{41} vs. $\sin^2 2\theta_{ee}$ parameter space for the scenario of ν_e disappearance only. Figure 14 shows the exclusion and sensitivity contours in the Δm^2_{41} vs. $\sin^2 2\theta_{\mu e}$ parameter space for the scenario of ν_e appearance only. Because there is an overall deficit (less than 2σ) in the data for ν_e CC channels compared to the prediction of the 3ν hypothesis, the ν_e disappearance data exclusion limit in figure 13 is weaker than the sensitivity and the ν_e appearance data exclusion limit in figure 14 is more stringent than the sensitivity. Figure 15 shows the comparisons of our result with the allowed region of MiniBooNE [32] in the Δm^2_{41} vs. $\sin^2 2\theta_{\mu e}$ parameter space. The MiniBooNE result is for a ν_e appearance only oscillation analysis.

Figure 16 shows the exclusion and sensitivity contours in the Δm^2_{41} vs. $\sin^2 2\theta_{\mu\mu}$ parameter space for the scenario of ν_μ disappearance only. Because of the relatively large systematic uncertainty (weak constraints from the other channels), the frequentist method produces a significantly different result from that using the Wilks' theorem or other approximations. The data-to-MC shape difference in the inclusive ν_μ CC channel can allow for more 4ν oscillation parameter space leading to a much weaker data exclusion limit than the median sensitivity.
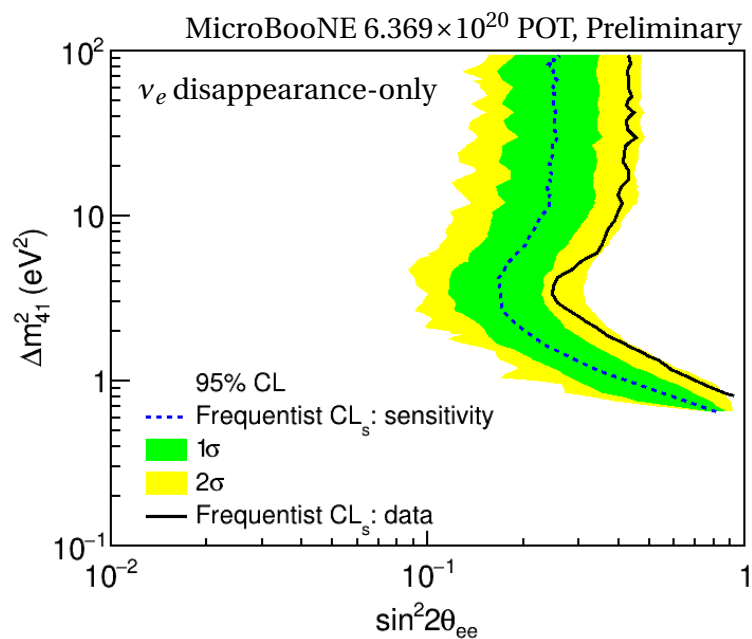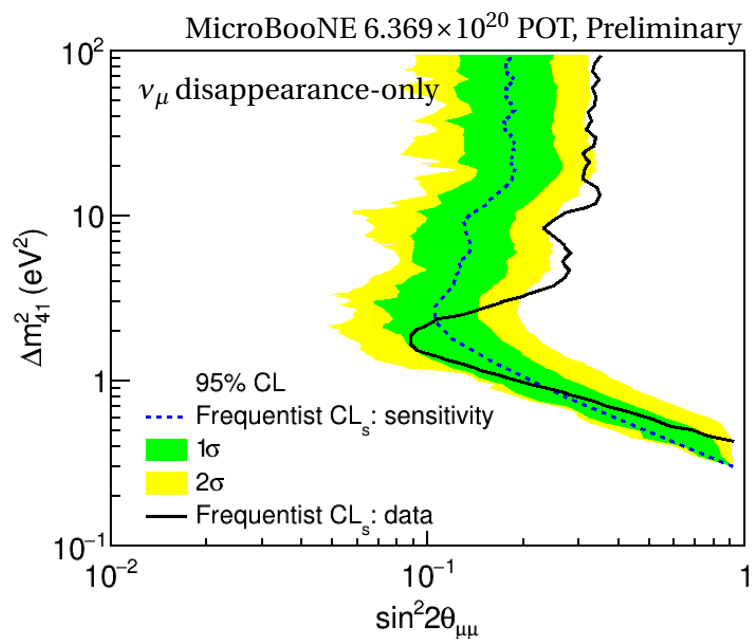
Figure 13: MicroBooNE 95% CL$_s$ sensitivity and data exclusion curves for ν_e disappearance-only. The solid black curve represents the exclusion contour. The blue dashed curve represents the sensitivity contour. Seven channels are used in the oscillation fit while only the ν_e disappearance oscillation effect is considered. The frequentist CLs sensitivity curve corresponds to the median value for each Δm_{41}^2 and the green/yellow bands correspond to 68.3% (1σ) and 95.5% (2σ) confidence levels.
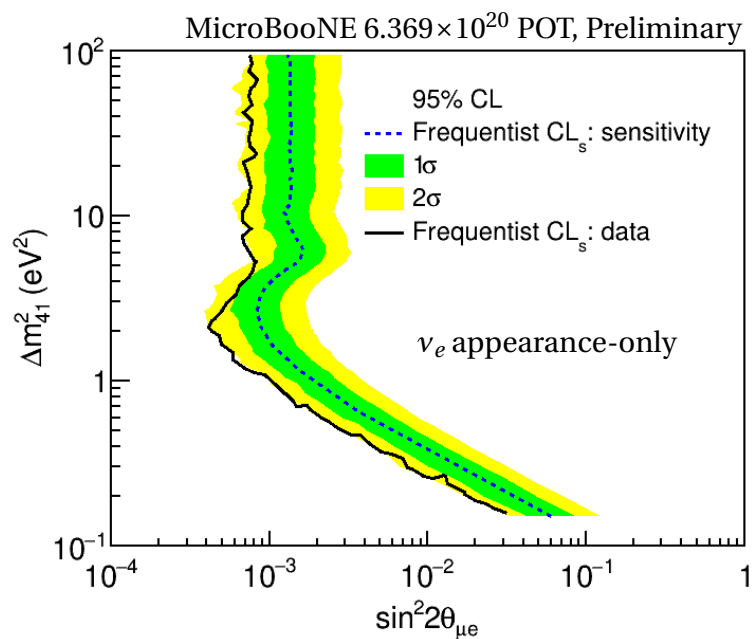
Figure 14: MicroBooNE 95% CL$_s$ sensitivity and data exclusion curves for ν_e appearance-only. The solid black curve represents the exclusion contour. The blue dashed curve represents the sensitivity contour. Seven channels are used in oscillation fit while only the ν_e appearance oscillation effect is considered. The frequentist CLs sensitivity curve corresponds to the median value for each Δm_{41}^2 and the green/yellow bands correspond to 68.3% (1σ) and 95.5% (2σ) confidence levels.
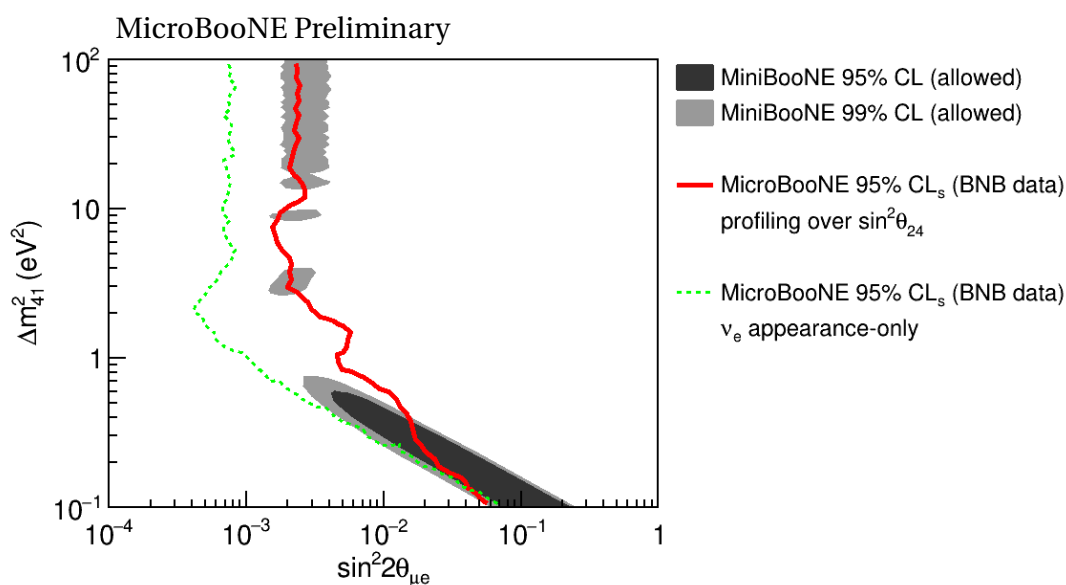
Figure 15: MicroBooNE 95% confidence level frequentist CL_s limits in the Δm_{41}^2 vs. $\sin^2 2\theta_{\mu e}$ parameter space. The MiniBooNE 95% and 99% CL allowed regions [32] are shown in the shaded areas, which were estimated from the ν_e appearance only scenario. The red solid curve represents the MicroBooNE 95% CL_s exclusion limit (2D profiling by minimizing over $\sin^2\theta_{24}$) in the full 3+1 neutrino oscillation scenario (both ν_e appearance and ν_e/ν_μ disappearance) using BNB Run 1-3 data. The green dashed curve represents the data exclusion limit in the ν_e appearance only scenario (physically not allowed by the 3+1 oscillation framework) as opposed to the full 3+1 oscillation result.

Figure 16: MicroBooNE 95% CL$_s$ sensitivity and data exclusion curves for ν_μ disappearance-only. The solid black curve represents the exclusion contour. The blue dashed curve represents the sensitivity contour. Seven channels are used in the oscillation fit while only the ν_μ disappearance oscillation effect is considered. The frequentist CLs sensitivity curve corresponds to the median value for each Δm_{41}^2 and the green/yellow bands correspond to 68.3% (1σ) and 95.5% (2σ) confidence levels.

REFERENCES

[1] P. Adamson et al. Improved Constraints on Sterile Neutrino Mixing from Disappearance Searches in the MINOS, MINOS+, Daya Bay, and Bugey-3 Experiments. *Phys. Rev. Lett.*, 125(7):071801, 2020, 2002.00301.

[2] M. Andriamirado et al. Improved short-baseline neutrino oscillation search and energy spectrum measurement with the PROSPECT experiment at HFIR. *Phys. Rev. D*, 103(3):032001, 2021, 2006.11210.

[3] F. Kaether, W. Hampel, G. Heusser, J. Kiko, and T. Kirsten. Reanalysis of the GALLEX solar neutrino flux and source experiments. *Phys. Lett. B*, 685:47–54, 2010, 1001.2731.

[4] V. V. Barinov et al. Results from the Baksan Experiment on Sterile Transitions (BEST). 9 2021, 2109.11482.

[5] J. N. Abdurashitov et al. Measurement of the solar neutrino capture rate with gallium metal. III: Results for the 2002–2007 data-taking period. *Phys. Rev. C*, 80:015807, 2009, 0901.2200.

[6] G. Mention, M. Fechner, Th. Lasserre, Th. A. Mueller, D. Lhuillier, M. Cribier, and A. Letourneau. The Reactor Antineutrino Anomaly. *Phys. Rev. D*, 83:073006, 2011, 1101.2755.

[7] Patrick Huber. On the determination of anti-neutrino spectra from nuclear reactors. *Phys. Rev. C*, 84:024617, 2011, 1106.0687. [Erratum: Phys.Rev.C 85, 029901 (2012)].

[8] Th. A. Mueller et al. Improved Predictions of Reactor Antineutrino Spectra. *Phys. Rev. C*, 83:054615, 2011, 1101.2663.

[9] A. P. Serebrov et al. Search for sterile neutrinos with the Neutrino-4 experiment and measurement results. *Phys. Rev. D*, 104(3):032003, 2021, 2005.05301.

[10] A. Aguilar-Arevalo et al. Evidence for neutrino oscillations from the observation of $\bar{\nu}_e$ appearance in a $\bar{\nu}_\mu$ beam. *Phys. Rev. D*, 64:112007, 2001, hep-ex/0104049.

[11] A. A. Aguilar-Arevalo et al. Improved Search for $\bar{\nu}_\mu \to \bar{\nu}_e$ Oscillations in the MiniBooNE Experiment. *Phys. Rev. Lett.*, 110:161801, 2013, 1303.2588.

[12] A. A. Aguilar-Arevalo et al. Updated MiniBooNE neutrino oscillation results with increased data and new background studies. *Phys. Rev. D*, 103(5):052002, 2021, 2006.16883.

[13] F. P. An et al. Evolution of the Reactor Antineutrino Flux and Spectrum at Daya Bay. *Phys. Rev. Lett.*, 118(25):251801, 2017, 1704.01082.

[14] F. P. An et al. Antineutrino energy spectrum unfolding based on the Daya Bay measurement and its applications. *Chin. Phys. C*, 45(7):073001, 2021, 2102.04614.

[15] M. Estienne et al. Updated Summation Model: An Improved Agreement with the Daya Bay Antineutrino Fluxes. *Phys. Rev. Lett.*, 123(2):022502, 2019, 1904.09358.

[16] C. Giunti, Y. F. Li, C. A. Ternes, and Z. Xin. Reactor antineutrino anomaly in light of recent flux model refinements, 10 2021, 2110.06820.

[17] Carlo Giunti and T. Lasserre. eV-scale Sterile Neutrinos. *Ann. Rev. Nucl. Part. Sci.*, 69:163–190, 2019, 1901.08330.

[18] R. Acciarri et al. Design and Construction of the MicroBooNE Detector. *JINST*, 12(02):P02017, 2017.

[19] T. Briese et al. Testing of Cryogenic Photomultiplier Tubes for the MicroBooNE Experiment. *JINST*, 8:T07005, 2013.

[20] P. Abratenko et al. Search for an Excess of Electron Neutrino Interactions in MicroBooNE Using Multiple Final State Topologies. 10 2021, 2110.14054.

[21] P. Abratenko et al. Search for an anomalous excess of charged-current quasi-elastic ν_e interactions with the MicroBooNE experiment using Deep-Learning-based reconstruction. 10 2021, 2110.14080.

[22] P. Abratenko et al. Search for an anomalous excess of charged-current ν_e interactions without pions in the final state with the MicroBooNE experiment. 10 2021, 2110.14065.

[23] P. Abratenko et al. Search for an anomalous excess of inclusive charged-current ν_e interactions in the MicroBooNE experiment using Wire-Cell reconstruction. 10 2021, 2110.13978.

[24] P. Abratenko et al. New $CC0\pi$ GENIE model tune for MicroBooNE. *Phys. Rev. D*, 105(7):072001, 2022, 2110.14028.

[25] Baobiao Yue, Wei Li, Jiajie Ling, and Fanrong Xu. A compact analytical approximation for a light sterile neutrino oscillation in matter. *Chin. Phys. C*, 44(10):103001, 2020, 1906.03781.

[26] Xiangpan Ji, Wenqiang Gu, Xin Qian, Hanyu Wei, and Chao Zhang. Combined Neyman–Pearson chi-square: An improved approximation to the Poisson-likelihood chi-square. *Nucl. Instrum. Meth. A*, 961:163677, 2020, 1903.07185.

[27] Alexander L. Read. Modified frequentist analysis of search results (The CL(s) method). In *Workshop on Confidence Limits*, pages 81–101, 8 2000.

[28] Thomas Junk. Confidence level computation for combining searches with small statistics. *Nucl. Instrum. Meth. A*, 434:435–443, 1999, hep-ex/9902006.

[29] X. Qian, A. Tan, J. J. Ling, Y. Nakajima, and C. Zhang. The Gaussian CL$_s$ method for searches of new physics. *Nucl. Instrum. Meth. A*, 827:63–78, 2016, 1407.5052.

[30] Glen Cowan, Kyle Cranmer, Eilam Gross, and Ofer Vitells. Asymptotic formulae for likelihood-based tests of new physics. *Eur. Phys. J. C*, 71:1554, 2011, 1007.1727. [Erratum: Eur.Phys.J.C 73, 2501 (2013)].

[31] Gary J. Feldman and Robert D. Cousins. A Unified approach to the classical statistical analysis of small signals. *Phys. Rev. D*, 57:3873–3889, 1998, physics/9711021.

[32] A. A. Aguilar-Arevalo, B. C. Brown, J. M. Conrad, R. Dharmapalan, A. Diaz, Z. Djurcic, D. A. Finley, R. Ford, G. T. Garvey, S. Gollapinni, A. Hourlier, E.-C. Huang, N. W. Kamp, G. Karagiorgi, T. Katori, T. Kobilarcik, K. Lin, W. C. Louis, C. Mariani, W. Marsh, G. B. Mills, J. Mirabal-Martinez, C. D. Moore, R. H. Nelson, J. Nowak, I. Parmaksiz, Z. Pavlovic, H. Ray, B. P. Roe, A. D. Russell, A. Schneider, M. H. Shaevitz, H. Siegel, J. Spitz, I. Stancu, R. Tayloe, R. T. Thornton, M. Tzanov, R. G. Van de Water, D. H. White, and E. D. Zimmerman. Updated miniboone neutrino oscillation results with increased data and new background studies. *Phys. Rev. D*, 103:052002, Mar 2021.

[33] C. A. Argüelles, I. Esteban, M. Hostert, Kevin J. Kelly, J. Kopp, P. A. N. Machado, I. Martinez-Soler, and Y. F. Perez-Gonzalez. MicroBooNE and the ν_e Interpretation of the MiniBooNE Low-Energy Excess. 11 2021, 2111.10359.